Luminescent Properties of Divalent Samarium-Doped Strontium Hexaborate

Qinghua Zeng,* Zhiwu Pei, Shubing Wang, and Qiang Su

*Laboratory of Rare Earth Chemistry and Physics, Changchun Institute of Applied Chemistry,
Chinese Academy of Sciences, Changchun, 130022, P. R. China*

Shaozhe Lu

*Laboratory of Excited-State Processes, Chinese Academy of Sciences,
Changchun, 130021, P. R. China*

The valence change of samarium from trivalent to divalent in strontium hexaborate (SrB_6O_{10}) prepared in air is observed. The temperature dependence of the luminescence and vibronic transitions of Sm^{2+} are studied. The Sm^{2+} ions occupy three crystallographic sites. With increasing temperature, the $^5D_0 \rightarrow {}^7F_0$ transition line exhibits red shifts, and the half-width increases. At room temperature, due to the thermal population through the $4f^5 5d$ channel, the $^5D_1 \rightarrow {}^7F_J$ transitions are observed even though the vibrational energy is very close to the energy gap between the $^5D_1$ and $^5D_0$ levels in the host. A coupled phonon energy of about 108 cm^{-1} is determined from the vibronic transitions of Sm^{2+} in the host.

Introduction

Strontium tetraborate, SrB_4O_7, is reported to be a very suitable host lattice for the luminescent divalent rare earth ions, such as Eu^{2+}, Sm^{2+}, Yb^{2+} and Tm^{2+},[1−4] and these divalent ions can be very stable even when heated in air at high temperature.[5−6] This is attributed to the structural framework: in SrB_4O_7, all the boron atoms are tetrahedrally coordinated with oxygen atoms and form a three-dimensional borate network.[7] The divalent ions in SrB_4O_7 are completely surrounded by the tetrahedral BO_4 units of the $(B_4O_7)_\infty$ network and therefore are hardly expected to be attacked by oxygen.[8] It was reported that the compound SrB_6O_{10} consists of BO_3 and BO_4 units on the basis of its infrared spectral data[9−11] and the Mn^{2+} could retain its divalent state even when prepared in air in this host.[12] These statements prompt us to investigate samarium-doped SrB_6O_{10}, and it may also be expected that Sm^{3+} can be reduced to Sm^{2+} prepared in air. On the other hand, since no detailed structure of SrB_6O_{10} was reported so far,[9,10] we therefore use the $^5D_0 \rightarrow {}^7F_0$ transition of Sm^{2+} in this host as structural probe to study the number of the crystallographic sites and their symmetries. The ionic radius of Sm^{2+} is very close to that of Sr^{2+} and both ions have the same valence, so some Sr^{2+} can be replaced by Sm^{2+} without serious distortion in the structure.

In this paper, the reduction process for samarium from trivalent to divalent is reported. The luminescence of Sm^{2+} in this host is also studied as a function of temperature.

Experimental Section

The preparation of the Sm^{2+}-activated SrB_6O_{10} was carried out according to the literature[9] but heated at 700 °C[13] since we did not obtain a well-crystallized sample at 800 °C. However, it can still be found that the sample contains a more or less vitreous phase from its X-ray diffraction patterns, as reported in the literatures.[9−11,14,15] The mixtures were heated in air or in a hydrogen−nitrogen (5% H_2) atmosphere.

The dopant Sm_2O_3 concentration is 2 mol % of the Sr^{2+} ions in the host compound. The structure of the sample was checked on a Rigaku D/MAX-IIB X-ray powder diffractometer, using Cu $K\alpha_1$ radiation. The structure of the sample is in good agreement with the JCPDS No. 20-1190.

The low-resolution photoluminescence measurements were measured on a SPEX DM3000f spectrofluorometer equipped with 0.22 m SPEX 1680 double monochromators (resolution 0.1 nm) and a 450 W xenon lamp as excitation source. The high-resolution emission spectra and lifetime were recorded with a Spex-1403 spectrophotometer under the excitation of a N_2 laser beam (337.1 nm) (National Research Instruments Co.) with the flow cryostat of gaseous helium. The temperature can be varied from 10 to 300 K. The high-temperature luminescence is recorded by an MPF-4 spectrofluorometer with a 150

(1) Meijerink, A.; Nuyten, J.; Blasse, G. *Lumin.* **1989**, *44*, 19.
(2) Lacam, A.; Chateau, G. *J. Appl. Phys.* **1989**, *66*, 366.
(3) Blasse, G.; Dirksen, G. J.; Meijerink, A. *Chem. Phys. Lett.* **1990**, *167*, 41.
(4) Schipper, W. J.; Meijerink, A.; Blasse, G. *J. Lumin.* **1994**, *62*, 55.
(5) Pei, Z.; Su, Q.; Zhang, J. J. *Alloys. Compd.* **1993**, *198*, 51.
(6) Peterson, J. R.; Xu, W.; Dai, S. *Chem. Mater.* **1995**, *7*, 1686.
(7) Perfoff, A.; Block, S. *Acta Crystallogr.* **1966**, *20*, 274.
(8) Machida, K.; Adachi, G.; Shiokawa, J. *Acta Crystallogr.* **1980**, *B36*, 2008.
(9) Chenot, C. F. *J. Am. Cerem. Soc.* **1967**, *50*, 117.
(10) Weir, C. E.; Schreoder, R. A. *J. Res. NBS.* **1964**, *68A*, 465.
(11) Machida, K.; Adachi G.; Shiokawa, J. *J. Lumin.* **1979**, *21*, 101.
(12) Koskentalo, T.; Leskela, M.; Niinisto, L. *Mate. Res. Bull.* **1985**, *20*, 265.

(13) Tews, W.; Becker, P.; Herzog, G.; Kunzler, G. *Z. Phys. Chem. (Leipzig)* **1987**, *268*, 985.
(14) Schipper, W.; van de Voort, D.; van de Berg, P.; Vroon, Z. A. E. P.; Blasse, G.; *Mate. Chem. Phys.* **1993**, *33*, 311.
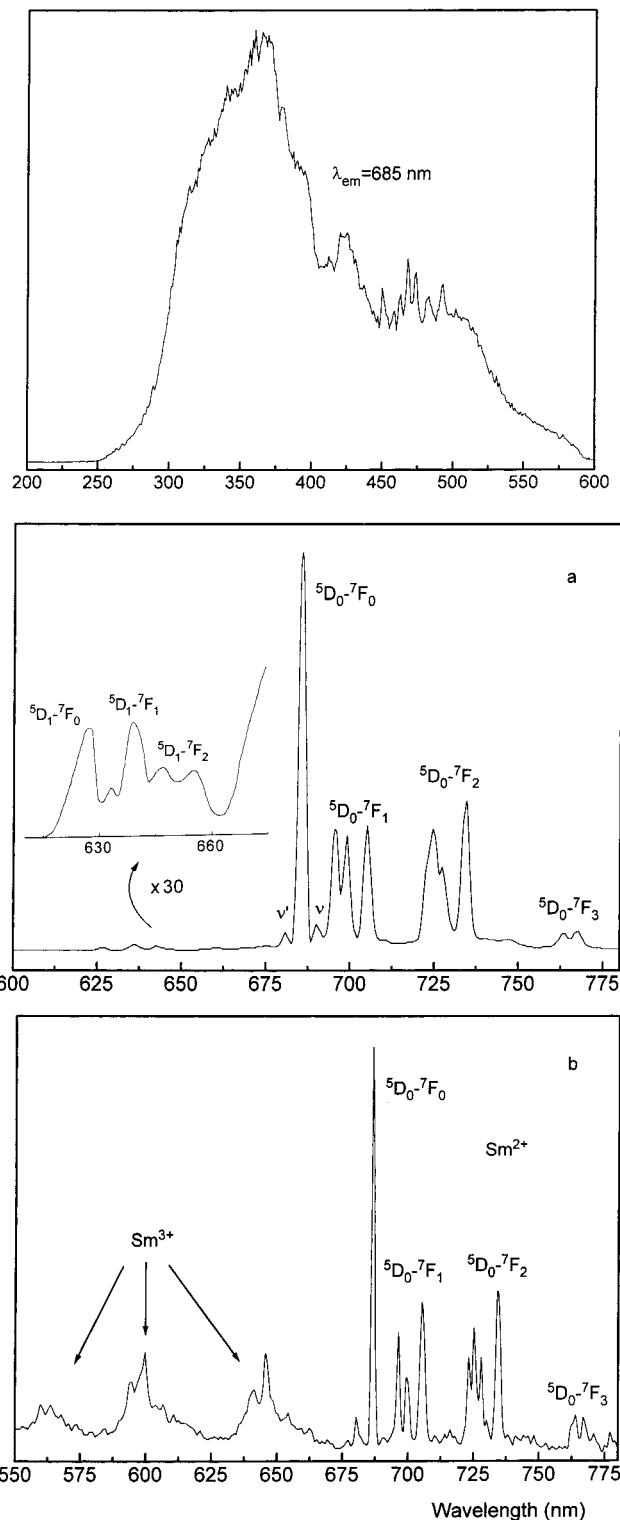(15) Leskla, M.; Koskentalo, T.; Blasse, G. *J. Solid State Chem.* **1985**, *59*, 272.

W xenon lamp as excitation source and a self-assembled furnace as heating source. The temperature can be varied in the range from 300 to 573 K.

Results and Discussion

1. The Low-Resolution Luminescence of Sm^{2+} in SrB_6O_{10}. The low-resolution emission and excitation spectra at room temperature of Sm^{2+} in SrB_6O_{10} prepared in H_2/N_2 and air are shown in Figure 1. The emission spectra shows that the luminescence of Sm^{2+} in SrB_6O_{10} prepared in air is identical to those prepared in H_2/N_2. Both consist of four groups of lines at 685, 700, 725, and 760 nm that correspond to the $^5D_0 \rightarrow {}^7F_J$ ($J = $ 0, 1, 2, 3) transitions in Sm^{2+}, respectively. The dominant line is at about 685 nm, which shows that the Sm^{2+} ions occupy the crystallographic sites without central symmetry in the host. A group of weak lines at 562, 600, and 647 nm correspond to $^4G_{5/2} \rightarrow {}^6H_J$ ($J = {}^5/_2$, $^7/_2$, $^9/_2$, respectively) transitions in Sm^{3+} ions when the sample was prepared in air. It is therefore deduced that the Sm^{3+} could be reduced to the divalent state in SrB_6O_{10} prepared at high temperature in air.

The excitation of divalent samarium takes place via strong $4f^5 5d$ absorption bands from which the ions quickly decay to the lower metastable level $^5D_0$ ($4f^6$). The excitation band consists of two bands with a maximum at about 364 and 485 nm, respectively, together with some sharp lines in the band. The crystal field splitting energy is about 6800 cm^{-1}, which is very close to the crystal field splitting energy of the 5d level in cubic coordination:[16] $\sim$7000 cm^{-1}. In cubic coordination, the 5d level is split into a lower e_g and a higher t_{2g} level. From the position of two excitation bands, it is suggested that the $4f^5 5d$ levels of Sm^{2+} in SrB_6O_{10} be located in the relatively higher energy position than in the alkaline earth halides.[17-19] The lines in the excitation spectrum correspond to the ^6H_J ($J = {}^{13}/_2$, $^{11}/_2$, $^9/_2$, $^7/_2$) states of the splitting of the $4f^5$ configuration.[20]

2. The High-Resolution Emission Spectra of Sm^{2+} and the Temperature Dependence. The high-resolution emission spectra at different temperatures were recorded since the temperature dependence of the relative intensities of the lines belonging to the same group is of great help to classify the lines according to the emitting Stark level. The intensity of the lines within each group is roughly evaluated from their heights. Figure 2 shows the high-resolution emission spectra at 10 K. Three groups of lines can be observed in the range from 14 586 to 14 519 cm^{-1}, 14 456 to 14 175 cm^{-1}, and 13 867 to 13 607 cm^{-1}, which correspond to the $^5D_0 \rightarrow {}^7F_0$, $^5D_0 \rightarrow {}^7F_1$, and $^5D_0 \rightarrow {}^7F_2$ transitions, respectively. Their positions and assignments are tabulated in Table 1. It should be noted that there are three lines in the $^5D_0 \rightarrow {}^7F_0$ transition at 14586, 14 566, and 14 519 cm^{-1} (designated I, II, and III in Figure 2) and nine lines in the $^5D_0 \rightarrow {}^7F_1$ transitions. If the
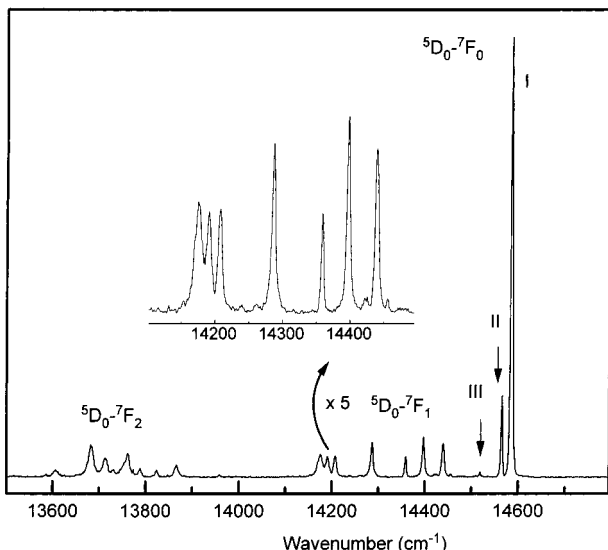
(16) Meijerink, A.; Dirksen, G. J. *J. Lumin.* **1995**, *63*, 189.
(17) Lauer, H. V. Jr.; Fong, F. K. *J. Chem. Phys.* **1976**, *65*, 3108.
(18) Gros, A.; Gaume, F.; Gacon, J. C. *J. Solid State Chem.* **1981**, *36*, 324.
(19) Sorokin, P. P.; Stenvenson, M. J.; Lank, J. R.; Pettit, G. D. *Phys. Rev.* **1962**, *127*, 503.
(20) Dieke G. H. *Spectra and Energy Levels of Rare Earth Ions in Crystals*; Crosswhite, H. M., Crosswhite, H., Eds.; Wiley: New York, 1968.

Figure 1. The low-resolution excitation spectra ($\lambda_{em} = 685$ nm) and emission spectra at room temperature of Sm^{2+} in SrB_6O_{10} prepared in (a) H_2/N_2 and (b) air ($\lambda_{ex} = 364$ nm). (The inset shows the enlargement of the emission in the range from 620 to 680 nm).

degeneracy of the $^7F_1$ energy level for one site is completely lifted and the lines are well-separated, the number of the lines is at most three. Therefore, Sm^{2+} ion must occupy at least three crystallographic sites in SrB_6O_{10} at 10 K. Our results confirm those reported in the literatures.[11,14,15] These authors reported data with the assumption that three crystallographic sites for Sr^{2+}

Figure 2. The high-resolution emission spectra of Sm^{2+} at 10 K in SrB_6O_{10}. (The inset shows the enlargement of the $^5D_0 \rightarrow ^7F_1$ transitions).

Table 1. Energetic Positions and Assignments of the Sm^{2+} Emission Spectra at 10 K in SrB_6O_{10}

| transitions ($^5D_0 \rightarrow ^7F_J$)[a]	wavenumber (cm^{-1})
$J = 0$	14 586
	14 566
	14 519
$J = 1$	14 456
	14 439
	14 422
	14 397
	14 359
	14 287
	14 208
	14 190
	14 175

[a] $J = 2$ transitions not resolved well.

are possible in the host. In center I and II, the $^5D_0 \rightarrow ^7F_0$ transition at 14 586 and 14 566 cm^{-1} has the strongest intensities, which shows that Sm^{2+} ions occupy the crystallographic sites without central symmetry. Because the $^5D_0 \rightarrow ^7F_2$ transition lines are not resolved well, it is difficult to derive information on the site symmetry of Sm^{2+} in this host.

Figure 3 shows the high-resolution emission spectra of Sm^{2+} at 100 and 250 K in the matrix. Some differences can be found in Figures 2 and 3. First, the intensities of center II to center I increase with increasing temperature, while that of center III decreases and is completely quenched at room temperature. These show that the energy transfer from center III to centers I and II may occur. Second, in the $^5D_0 \rightarrow ^7F_1$ transitions, three lines at 14 456, 14 439, and 14 422 cm^{-1} vanishes at 250 K. Therefore, these three lines must be assigned to center III. In center III, the $^5D_0 \rightarrow ^7F_1$ transitions at 14 439 cm^{-1} has the strongest intensity. Therefore, the site symmetry of Sm^{2+} in the third crystallographic site must be different from those in the other two sites. For center III, the Sm^{2+} ion must occupy a site with central symmetry.

The temperature dependence of the energy transfer processes among different Sm^{2+} centers and the integrated emission intensities of the Sm^{2+} $^5D_0 \rightarrow ^7F_0$ transition in centers I and II were measured as a function of
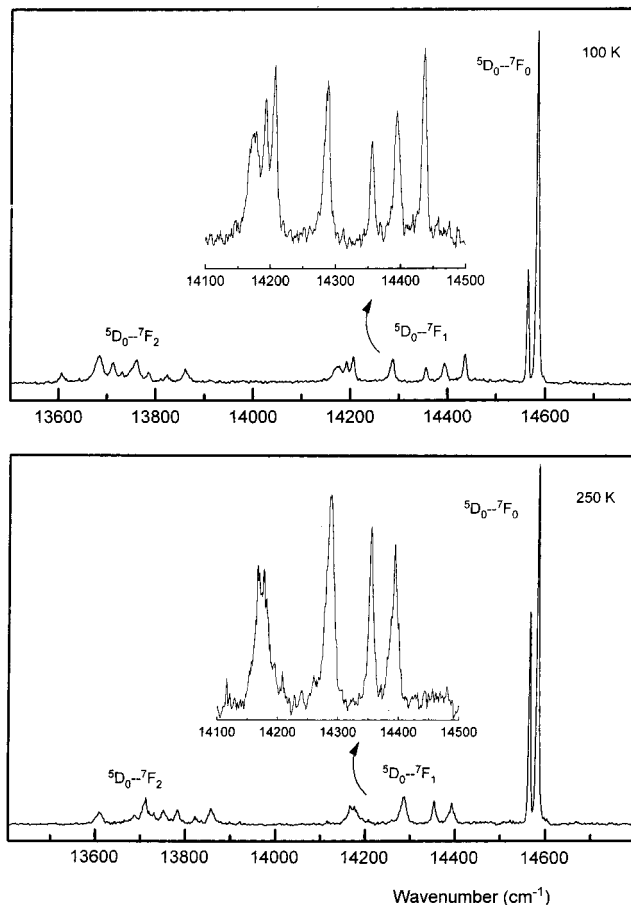

Figure 3. The high-resolution emission spectra of Sm^{2+} at 100 and 250 K in SrB_6O_{10}. (The inset shows the enlargement of the $^5D_0 \rightarrow ^7F_1$ transitions.)
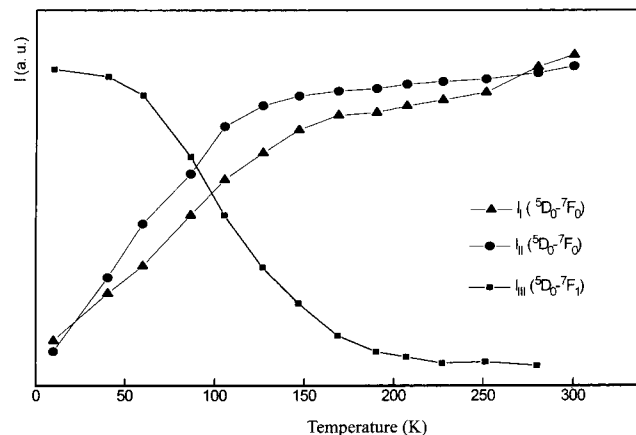
Figure 4. The temperature dependence of the intensities of the Sm^{2+} $^5D_0 \rightarrow ^7F_0$ transition in center I (I_I), center II (I_{II}) and of $^5D_0 \rightarrow ^7F_1$ in center III (I_{III}) in SrB_6O_{10}.

temperature in the range from 10 to 300 K. The emission intensity of the Sm^{2+} $^5D_0 \rightarrow ^7F_0$ transition in center III is too weak to be measured, therefore, we only measure the intensities of the $^5D_0 \rightarrow ^7F_1$ transitions at 14 456, 14 439, and 14 422 cm^{-1}. The results are shown in Figure 4. The intensities for centers I and II increase between 10 and 200 K and finally decrease between 200 and 300 K, while those of center III decrease with increasing temperature and are almost quenched at about 200 K. The energy transfer processes were also observed in the luminescence of the divalent europium
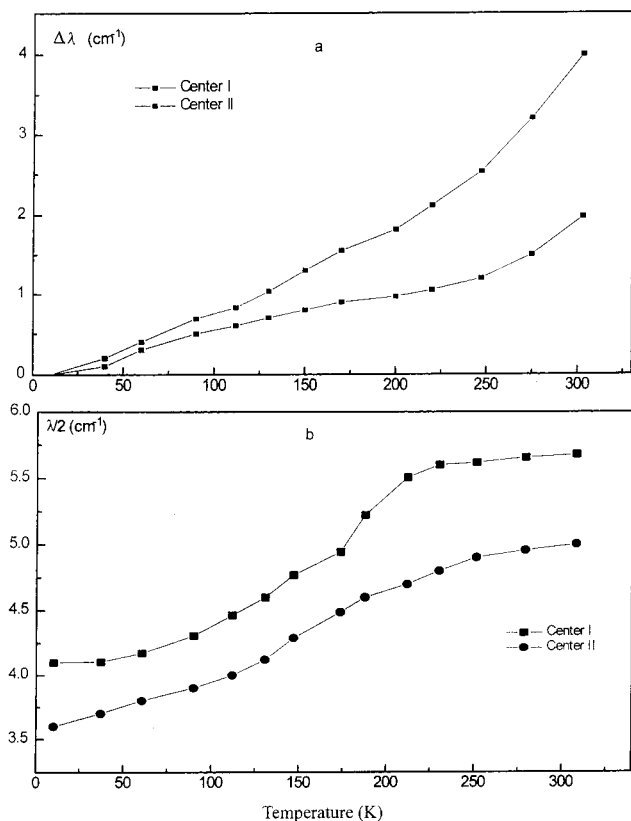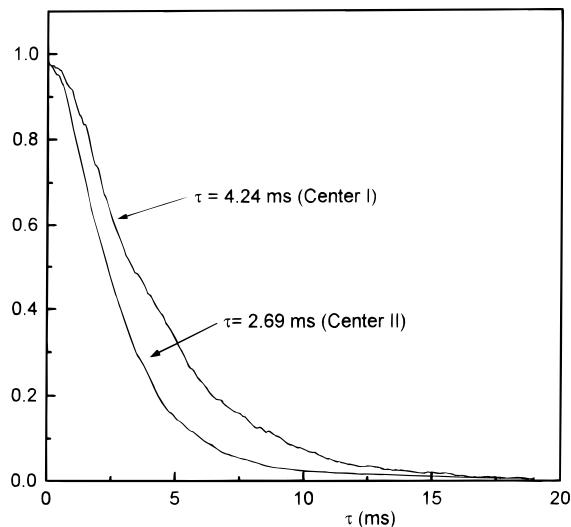
Figure 5. The temperature dependence of the line shift (a) and the half-width (b) of the Sm^{2+} $^5D_0 \rightarrow ^7F_0$ transition in center I, center II in SrB_6O_{10}.

Figure 6. The decay curves of the Sm^{2+} $^5D_0 \rightarrow ^7F_0$ transition in centers I and II at 300 K in SrB_6O_{10}.

Figure 7. The temperature dependence of the lifetime of the Sm^{2+} $^5D_0 \rightarrow ^7F_0$ transition in center I in SrB_6O_{10}.

in this matrix.[14] In SrB_6O_{10}:Eu^{2+}, energy transfer occurs from center III to centers II and I with increasing temperature, and the emission of Eu^{2+} in center III is quenched at 150 K, which is very close to the Sm^{2+} quenching temperature at 200 K in the same host. In a qualitative way, the temperature effects on the intensities of the Sm^{2+} $^5D_0 \rightarrow ^7F_0$ transition can be illustrative for the temperature dependence of the energy transfer process between two centers. It is caused by the need for the phonon assistance in the energy transfer process.

The thermal effects on the line shift and the half-width of the Sm^{2+} $^5D_0 \rightarrow ^7F_0$ transition (centers I and II) in SrB_6O_{10} at different temperatures are studied between 10 and 300 K. The results are shown in Figure 5. It can be found that the positions of the $^5D_0 \rightarrow ^7F_0$ transition lines in both centers undergo red shifts as temperature increases. The half-width also increase with increasing temperature due to the thermal broadening. The thermal effects on line shift should be due to the metastable state of the $4f^5 5d$ configuration within Sm^{2+}, since the electronic charge is strongly affected by the thermal perturbations of the environment. The thermal broadening is due to static and random microscopic strains and Raman scattering of phonons.

The lifetime measurements can also yield information about the kinetic of the luminescence process, such as the fluorescence efficiency, energy transfer, and the excitation and deexcitation process. The decay processes of the Sm^{2+} $^5D_0 \rightarrow ^7F_0$ transitions in center I and II in SrB_6O_{10} are single exponential in the temperature range from 10 to 300 K. At 10 K, the lifetime of the Sm^{2+} $^5D_0 \rightarrow ^7F_0$ transition for centers I and II is almost the same: $\tau_I \approx 5.0$ ms, $\tau_{II} \approx 4.5$ ms, whereas at 300 K, the
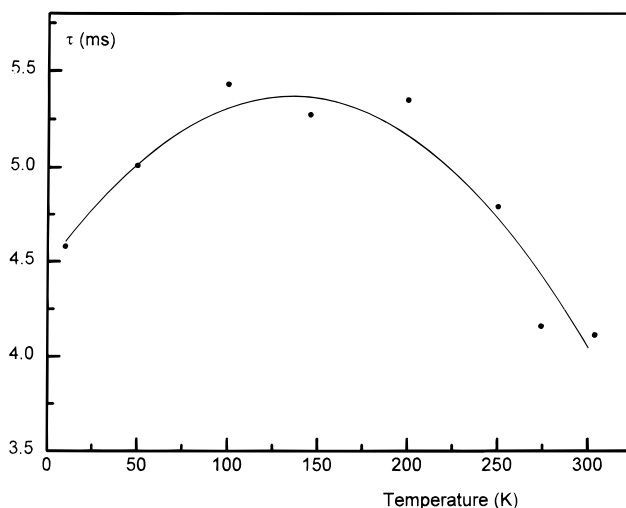
lifetime for these two centers is 4.24 and 2.69 ms, respectively (Figure 6). These results show that the different lifetimes originate from different luminescent centers.

The dependencies of the lifetime of center I of Sm^{2+} in SrB_6O_{10} as a function of temperature in the range from 10 to 300 K are shown in Figure 7. The decay time of Sm^{2+} in center I is temperature dependent. Between 10 and 200 K, the lifetime slightly increases with increasing temperature. This is possibly because of the energy transfer from center III to centers II and I. At around 200 K, the lifetime starts to decrease with increasing temperature due to the thermal depopulation in the $^5D_0$ level. The effects of temperature on lifetime is in agreement with those on the intensities, as discussed above. However, the complicated interactions among three luminescent centers are a deterrent for us to reach a further view on the kinetics of the luminescence process for Sm^{2+} in SrB_6O_{10}.

3. The Vibronic Transitions of Sm^{2+}. From Figure 1, it can be found that there are two weak lines beside the $^5D_0 \rightarrow ^7F_0$ transition (14586 cm^{-1}): one is at 680.3 nm (14 699 cm^{-1}, denoted ν') and other is at 690.4 nm

(14 484 cm^{-1}, denoted ν). Since these extra lines are weak and broad and there are only three sites for Sm^{2+}, they cannot be the transitions of Sm^{2+} but instead the vibronic transitions (phonon satellite lines). These vibronic transitions are caused by the interactions between the electrons and the lattice. The electrons are coupled with the zero-phonon line (ZPL) $^5D_0 \rightarrow {}^7F_0$ during the transition between these two energy levels. The energy difference between ν' and the ZPL is $\hbar\omega_{\nu'} \approx 113$ cm^{-1} and that for ν is about $\hbar\omega_\nu \approx 104$ cm^{-1}. This vibration is a vibrational mode in which Sm moved relative to the borate group. These phonon satellite lines originated from the transition in which the $^5D_0$ and $^7F_0$ states have different lattice vibration levels. Lines ν and ν' are attributed to the transitions $|^5D_0, n\rangle \rightarrow |^7F_0, n+1\rangle$ ($P = 1$ for emitting P phonons) and $|^5D_0, n+1\rangle \rightarrow |^7F_0, n\rangle$ ($P = -1$ for absorbing P phonons), respectively, where n is the quantum number of vibration levels of the crystal lattice.

For f–f transition of rare earth ions, since the 4f electrons are well-shielded by the outer 5s^2 and 5p^6 electrons, the coupling of the transitions within the 4f^n configuration with vibrations is weak and then the intensity ratio of ν and ν' to $^5D_0 \rightarrow {}^7F_0$ zero-phonon line can be calculated as:[21-25]

$$I_{\nu'}/I_0 = S\langle 1+m\rangle = \frac{S}{1-\exp\left(\frac{-\hbar\omega}{kT}\right)} \quad P=1 \quad (1a)$$

$$I_{\nu}/I_0 = S\langle m\rangle = \frac{S\exp\left(\frac{-\hbar\omega}{kT}\right)}{1-\exp\left(\frac{-\hbar\omega}{kT}\right)} \quad P=-1 \quad (1b)$$

where k is the Boltzmann constant; S is the Huang–Rhys factor, which shows the coupling strength during the transitions; $\langle m\rangle$ is Plank's thermal average quantum index, $\langle m\rangle = [\exp(-\hbar\omega/kT)/[1-\exp(-\hbar\omega/kT)]$; T is absolute temperature; and $\hbar\omega$ is the phonon energy. For the sample at room temperature (Figure 1), $\hbar\omega$ is taken from the average phonon energy: $\hbar\omega \approx 108$ cm^{-1}; $T = 300$ K, the ratio of I_ν/I_0 is about 0.013. From eq 1b, it can be calculated that the Huang–Rhys factor $S \approx 0.015$. Using this value and eq 1a, we can find $I_{\nu'}/I_0 \approx 0.037$, close to the experimental result $I_{\nu'}/I_0 \approx 0.033$.

The shape of the vibronic spectra is mainly governed by the electron–phonon interactions. If this interaction is weak, the spectra will be dominated by sharp lines. If this interaction is strong, then structureless bands are observed. In the f–f transitions of rare earth ions, this interaction is usually weak and sharp vibronic transition lines will appear.[25] But this is not always the case. The interaction will also change for different lattices. In the spectra of Sm^{2+} in BaCl$_2$ and BaBr$_2$, a wide vibronic sideband which stretches from ZPL to $\sim$200 cm^{-1} is found.[17] These vibronic sidebands are caused by the lattice vibrations in the anion sublattices. These continuous bands can be explained by the multiphonon-configuration-coordinate mechanism. In this mechanism, all of the vibrational modes in the lattice will be coupled with the transitions, which results in a wide continuous band. In SrB$_6$O$_{10}$:Sm^{2+}, we do not find such a continuous band but only sharp phonon lines are found beside ZPL. These can be explained well by the single-configuration-coordinate mechanism, in which only the vibration mode with single frequency is coupled with the 4f electrons, which results in sharp and weak lines.

At all temperatures below 300 K, no $^5D_1 \rightarrow {}^7F_J$ transitions are found, even at 10 K. This is contrast to the spectra of Sm^{2+} in BaCl$_2$, BaBr$_2$.[17] In these alkaline earth halides, Sm^{2+} shows the $^5D_1 \rightarrow {}^7F_J$ at lower temperature and is gradually quenched at higher temperature. These differences are owing to the different vibrational energy in the host lattice, which lead to different radiative and nonradiative transition rates from $^5D_1$ (4f^{5}5d) to $^5D_0$ levels. The nonradiative transition rate (A_{NR}) from $^5D_1$ to $^5D_0$ can be calculated by the following equation:[21-25]

$$A_{NR} = N\frac{(S\langle m+1\rangle)^{P_0}\exp(-S\langle 2m+1\rangle)}{P_0!} \quad (2)$$

where N is the rate constant of the nonradiative transition within the order of $10^{11}\sim 10^{14}$; $P_0 = (\Delta E_{10}/\hbar\omega_{max})$ (the number of the phonons bridging the energy difference ΔE_{10} between the level of $^5D_1$ and $^5D_0$,); and $\hbar\omega_{max}$ is the maximum phonon energy in the host lattice. $\hbar\omega_{max}$ changes in different host lattice, whereas ΔE_{10} ($\sim$1350 cm^{-1}) does not. In SrB$_6$O$_{10}$, $\hbar\omega_{max}$ is around $\sim$1200 cm^{-1} (the vibrational energy of BO$_3$ units[10]), so $P_0 \approx 1$, and then $A_{NR} \approx (4 \times 10^9)-(4 \times 10^{13})$. For the purpose of comparison, we take BaCl$_2$:Sm^{2+} as an example. In BaCl$_2$:Sm^{2+}, the phonon energy is $\hbar\omega_{max} \approx 210$ cm^{-1}; therefore, $P_0 \approx 6-7$. Therefore, the nonradiative transition rate from $^5D_1$ to $^5D_0$ level in SrB$_6$O$_{10}$ is about 10^7-10^{15} times higher than in BaCl$_2$. This comparison reveals that no optical transition from $^5D_1$ to ^7F_J levels is found, even at 10 K for Sm^{2+} in SrB$_6$O$_{10}$, while those transitions can still be observed even at 77 K for Sm^{2+} in BaCl$_2$.[17]

However, an interesting phenomenon is that some weak sharp lines in the range from 620 to 670 nm are observed at room temperature (see Figure 1). These lines must correspond to the $^5D_1 \rightarrow {}^7F_J$ ($J = 0, 1, 2$) transitions of Sm^{2+} in SrB$_6$O$_{10}$. At first glance, these results conflict with the discussions above and also conflict with the usual observation that, generally, the $^5D_1 \rightarrow {}^7F_J$ transitions are previously quenched by temperature before the $^5D_0 \rightarrow {}^7F_J$ transitions (two-step fluorescence quenching mechanism). The observation of the $^5D_1 \rightarrow {}^7F_J$ transitions at room temperature can be explained by the $^5D_1$ level being thermally populated by the $^5D_0$ level via the 4f^{5}5d level, and therefore, the transition sequence becomes $^5D_0 \rightarrow {}^5D_1 \rightarrow {}^7F_J$. The indirect $^5D_1 \rightarrow {}^5D_0$ nonradiative channel through the 5d band was considered to be a novel situation, and a direct $^5D_1 \rightarrow {}^5D_0$ coupling should be the more likely event due to the relatively close proximity of these two J levels.[17]

4. High-Temperature Emission Spectra of Sm^{2+}. Under the excitation of 254 nm radiation, the sample SrB$_6$O$_{13}$:Sm^{2+} emits deep red light at room temperature, whereas it emits yellow light at high temperature. This
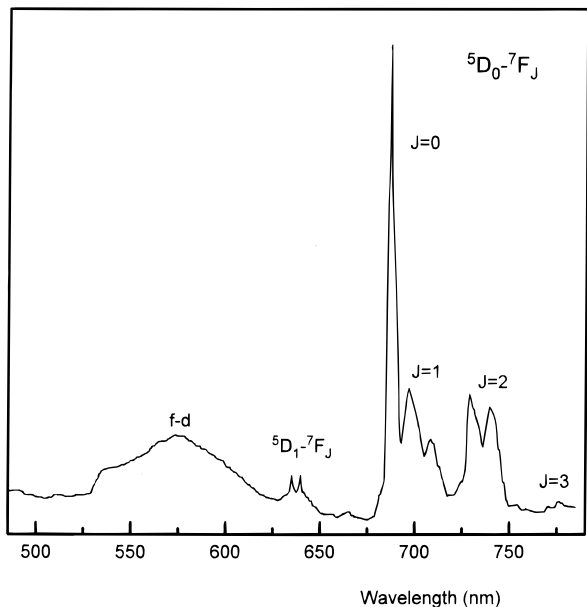
(21) Huang, K.; Rhys, A. *Proc. R. Soc. (London)* **1950**, *A204*, 406.
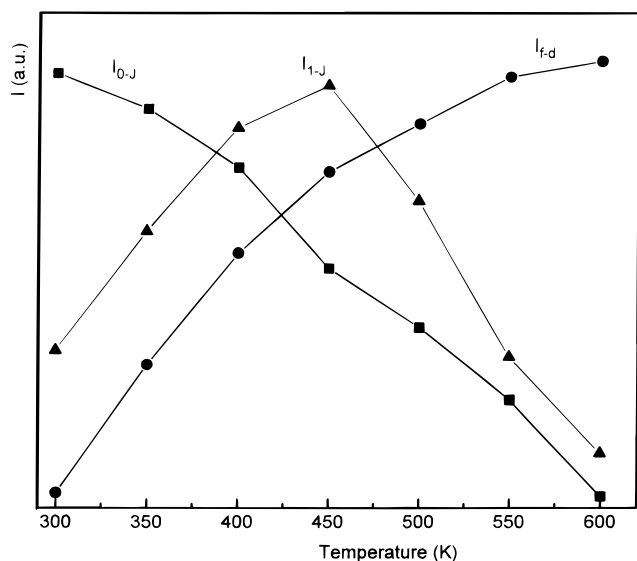(22) Pekar, S. *Zh. Eksp. Teor. Fiz.* **1950**, *20*, 510.
(23) Struck, C. W.; Fonger, W. H. *J. Chem. Phys.* **1974**, *60*, 1988.
(24) Huang K. *Progr. Phys.* **1981**, *1*, 31 (in Chinese).
(25) Blasse, G. *Int. Rev. Phys. Chem.* **1992**, *11*, 71.

Figure 8. The emission spectra of Sm^{2+} at 450 K in SrB_6O_{10}.

Figure 9. The temperature dependence of the intensities of the Sm^{2+} $^5D_1 \rightarrow ^7F_J$ (I_{1-J}), $^5D_0 \rightarrow ^7F_J$ (I_{0-J}), and $4f^55d \rightarrow ^7F_0$ (I_{f-d}) transitions in SrB_6O_{10}.

yellow light cannot be the mixture of the emission of Sm^{2+} and Sm^{3+} $^4G_{5/2} \rightarrow ^6H_J$ transitions, since it emits deep red light again when the sample is cooled to room temperature. Figure 8 shows the emission spectra of Sm^{2+} in SrB_6O_{10} at 450 K. The sample exhibits an intense broad band with maximum at about 580 nm. This broad band is characteristic of the Sm^{2+} $4f^55d \rightarrow ^7F_0$ electron-dipole-parity allowed transitions. The temperature dependence of the intensities of the Sm^{2+} $^5D_1$, $5D_0 \rightarrow ^7F_J$ and $4f^55d \rightarrow ^7F_0$ transitions is shown in Figure 9. The emission intensities of $^5D_0 \rightarrow ^7F_J$ transitions decrease with increasing temperature, whereas that of the $4f^55d \rightarrow 4f^6$ transition increase. The intensities of the $^5D_1 \rightarrow ^7F_J$ transitions increase at temperatures below $\sim$450 K, due to the thermal population from the $^5D_0$ level via the 5d band. At higher temperature, these transition intensities then decrease and are almost completely quenched at 573 K owing to its thermal nonradiative depopulation. The rapid decrease of $^5D_0$

fluorescence above 300 K is caused by a two-step quenching process through the 5d level, whereas the 5d level is thermally populated by $^5D_0$ and gives rise to a strong radiative transition to the ground state. Thus the yellow $4f^55d \rightarrow 4f$ broad band emission occurs at the expense of $^5D_0$ fluorescence. The yellow light, which is observed at high temperature, must be the combination of the Sm^{2+} $^5D_0 \rightarrow ^7F_0$ and $4f^55d \rightarrow 4f^6$ transitions. The $4f^5 5d \rightarrow 4f$ broad band is also observed in the spectra of Sm^{2+} in alkaline earth halides.[17,26] In different halides, the broad band appears at different temperature. This difference is caused by the different energy of the lowest-lying 5d level. The process for the $4f^55d \rightarrow 4f^6$ transition is the same as for the $^5D_1 \rightarrow ^7F_J$ transitions. Both of the $4f^55d$ and $^5D_1$ levels are thermally populated by the process $^5D_0 \rightarrow 4f^55d \rightarrow ^5D_1 \rightarrow ^7F_J$ and result in the $^5D_1 \rightarrow ^7F_J$ and $4f^55d \rightarrow 4f^6$ transitions. But because the $4f^55d \rightarrow 4f^6$ transition is an allowed one, its intensity is stronger than that of the $^5D_1 \rightarrow ^7F_J$ parity-forbidden transitions. The thermal depopulation of $^5D_0$ via the 5d band was also observed in alkaline earth halides.[17] This is an expected behavior since nonradiative coupling between $^5D_0$ and the highest-lying $^7F_6$ level is unlikely, due to the large energy gap between these two J levels ($\sim$10 500 cm^{-1}). The maximum phonon energies in SrB_6O_{10} are $\sim$1200 cm^{-1}. A nine-phonon transition cannot play a significant role in the decay of $^5D_0$ since it is known that the multiphonon relaxation is inefficient for more than a seven-phonon process.[17,26]

As the results above show, the thermal behavior of luminescence from the Sm^{2+} is predictably dependent on the phonon frequency of the host lattice. The luminescence of Sm^{2+} ions frequently results from the transitions between the $4f^n$ manifolds that are remote from the $4f^{n-1}5d$ states. The temperature variation of the Sm^{2+} luminescence is almost probably governed by the lowest lying $4f^55d$ states. The lowest lying energy level of $4f^55d$ will change in different lattices, and therefore, the f$\rightarrow$d transition occurs at different temperatures. When describing the temperature dependence of Sm^{2+} luminescence, the variable f$\rightarrow$d energy gaps as well as the usual dependence on the mediating phonon frequency must be taken into account.

Conclusions

The investigation on the valence change and luminescence of samarium ions in SrB_6O_{10} prepared in H_2/N_2 and air shows that the matrix SrB_6O_{10} is a good host for the divalent samarium ions. Sm^{3+} can be reduced to Sm^{2+} in SrB_6O_{10} prepared in air at high temperature. The luminescence of Sm^{2+} reveals that Sm^{2+} ions occupy at least three crystallographic sites in the host lattice: two of them are in the sites without central symmetry, whereas the other one has central symmetry. From 10 to 300 K, energy transfer occurs from center III to centers II and I with increasing temperature. A coupled phonon energy of about 108 cm^{-1} is determined from the vibronic transition of Sm^{2+}. The position of the $^5D_0 \rightarrow ^7F_0$ transition exhibits red shifts. The high-temperature emission spectra show that the $^5D_0 \rightarrow ^7F_J$ transition of Sm^{2+} decreases with increasing tempera-

(26) Fong, F. K. Lauer, H. V.; Chilver, C. R.; Miller, M. M. *J. Chem. Phys.* **1975**, *63*, 366.

ture while the 5d→4f broad band increases. In this temperature quenching process, the $^5D_0$ level is thermally depopulated by nonradiative deexcitation to the $4f^55d$ band and the $^5D_1$ level. The thermal population through the $4f^55d$ channel also causes the $^5D_1 \rightarrow {}^7F_J$ transitions, even though the vibrational energy is very close to the energy gap between the $^5D_1$ and $^5D_0$ levels in the host.

CM980479I